Palaeogeography, Palaeoclimatology, Palaeoecology 414 (2014) 403–414

Contents lists available at ScienceDirect

Palaeogeography, Palaeoclimatology, Palaeoecology

journal homepage: www.elsevier.com/locate/palaeo

Pliocene environmental change in West Africa and the onset of strong NE trade winds (ODP Sites 659 and 658)

Francesca Vallé [a], Lydie M. Dupont [a,*], Suzanne A.G. Leroy [b], Enno Schefuß [a], Gerold Wefer [a]

[a] MARUM — Center for Marine Environmental Sciences, University of Bremen, Leobenerstr, D28359 Bremen, Germany
[b] Institute for the Environment, Brunel University London, Uxbridge UB8 1QN, UK

ARTICLE INFO

Article history:
Received 4 June 2014
Received in revised form 10 September 2014
Accepted 24 September 2014
Available online 5 October 2014

Keywords:
Pollen
Pleistocene
Pliocene
NE trade winds
West Africa

ABSTRACT

Pliocene vegetation dynamics and climate variability in West Africa have been investigated through pollen and XRF-scanning records obtained from sediment cores of ODP Site 659 (18°N, 21°W). The comparison between total pollen accumulation rates and Ti/Ca ratios, which is strongly correlated with the dust input at the site, showed elevated aeolian transport of pollen during dusty periods. Comparison of the pollen records of ODP Site 659 and the nearby Site 658 resulted in a robust reconstruction of West African vegetation change since the Late Pliocene. Between 3.6 and 3.0 Ma the savannah in West Africa differed in composition from its modern counterpart and was richer in Asteraceae, in particular of the Tribus Cichorieae. Between 3.24 and 3.20 Ma a stable wet period is inferred from the Fe/K ratios, which could stand for a narrower and better specified mid-Pliocene (mid-Piacenzian) warm time slice. The northward extension of woodland and savannah, albeit fluctuating, was generally greater in the Pliocene. NE trade wind vigour increased intermittently around 2.7 and 2.6 Ma, and more or less permanently since 2.5 Ma, as inferred from increased pollen concentrations of trade wind indicators (*Ephedra*, *Artemisia*, *Pinus*). Our findings link the NE trade wind development with the intensification of the Northern Hemisphere glaciations (iNHG). Prior to the iNHG, little or no systematic relation could be found between sea surface temperatures of the North Atlantic with aridity and dust in West Africa.

1. Introduction

An understanding of the driving forces of Pliocene climate is the aim of many studies because the middle Pliocene may constitute a geological analogue for future climate (Salzmann et al., 2011; Fedorov et al., 2013). Most of the Pliocene (Zanclean and the beginning of the Piacenzian; 5.3–~3 Ma) was characterised by global mean annual temperatures 2–4 °C higher than in preindustrial times and estimated carbon dioxide concentrations were close to modern values of up to 400 ppm (Brierley et al., 2009; Bartoli et al., 2011).

Some authors claim that the so-called "permanent El Niño" state of the Pacific Ocean was one of the most important features of Pliocene warmth influencing the tropical atmosphere (Wara et al., 2005; Fedorov et al., 2006; Lawrence et al., 2006). The "permanent El Niño" is specified by a deep equatorial thermocline, a small east-to-west sea surface temperature (SST) gradient, and a reduced SST gradient between the equator and the tropics resulting in an expanded tropical warm pool in the Pacific Ocean with or without a reduced cold tongue of low equatorial SSTs (Brierley et al., 2009; Fedorov et al., 2013). These oceanic conditions would have had consequences for the atmospheric circulation in the Southern and Northern Hemispheres in the form of weaker Walker and Hadley cells (Brierley et al., 2009) implying reduced trade winds, which today contribute to create the asymmetry in the equatorial thermocline (Wara et al., 2005). Ocean–atmosphere conditions changed once the meridional temperature gradient started to increase and the tropical thermocline started to shoal (Fedorov et al., 2013). However, recent studies by O'Brian et al. (2014) and Zhang et al. (2014) question the temperature reconstructions of the West Pacific Warm Pool and Zhang et al. argue that the meridional SST gradient was already in existence in the Tortonian or Late Miocene (i.e. since 11.6 Ma).

A cooling trend indicated by heavier stable oxygen isotope values of benthic foraminifers (e.g. Lisiecki and Raymo, 2005) started at around ~3.3 Ma. Many studies reconstructing SST in the Pacific (Wara et al., 2005; Lawrence et al., 2006; Brierley et al., 2009; Etourneau et al., 2010) reveal an increase in the meridional gradient and suggest intensification of the Hadley cell during the cooling at the Pliocene–Pleistocene transition, although the proposed timing of events varies. During the cooling the Northern Hemisphere glaciations intensified (iNHG) and the Earth's system changed from a unipolar glaciated setting to the current bipolar glaciation with a circum-Arctic synchronous ice-sheet response after 2.7 Ma (cf. Jansen et al., 1996; Ravelo et al., 2004; De Schepper et al., 2014). The influence of obliquity on climate variability became stronger (Lisiecki and Raymo, 2005). A likely explanation for

* Corresponding author.
E-mail addresses: dupont@uni-bremen.de, ldupont@marum.de (L.M. Dupont), suzanne.leroy@brunel.ac.uk (S.A.G. Leroy).

http://dx.doi.org/10.1016/j.palaeo.2014.09.023

the cooling is the reduction of atmospheric carbon dioxide concentrations in the order of 100 ppm between 4 and 2 Ma (Bartoli et al., 2011; Fedorov et al., 2013). Moreover, the development of strong stratification in the subarctic Pacific Ocean could have resulted in both cooling in spring and enough moisture in fall to trigger the growth of large ice sheets in North America since 2.7 Ma (Haug et al., 1999, 2005).

The results of the iNHG are apparent in the North Atlantic by the southward diversion of the North Atlantic Current during glaciations (Naafs et al., 2010; Hennissen et al., 2014). These authors studied SSTs of the North Atlantic in combination with aeolian terrestrial input from North America. The supply of plant wax in the marine sediments strongly increased during every glacial since 2.7 Ma. Glacial erosion in North America would have released dust and wax of higher plants that were transported eastwards by west winds to the North Atlantic (Naafs et al., 2012).

Over the last 5 Ma the climate in Africa showed a long-term aridification trend starting around 3 Ma superimposed by alternating wet–dry cycles paced by orbital precession driving the monsoon system (Trauth et al., 2009). This trend resulted in a strong decline in tree cover in West Africa at 2.7 Ma as recorded in sediments offshore from the Niger Delta (Morley, 2000). Also in eastern Africa, vegetation became more steppe-like when grasslands expanded and aridity increased between 2.7 and 2.5 Ma (Bonnefille, 2010). Several studies proposed that the aridification in subtropical West Africa occurred parallel to the iNHG and with the intensification of northeast trade winds (deMenocal et al., 1993; Leroy and Dupont, 1994; Tiedemann et al., 1994; deMenocal, 2004; Bonnefille, 2010). Moreover, the intensification of the trade wind system had an impact on coastal upwelling systems. Marlow et al. (2000), studying the Benguela upwelling system along the southwest coast of Namibia, suggested that the intensification of trade winds started "a positive feedback cycle" which helped in removing CO_2 from the atmosphere and started its storage in the deep ocean, thus enhancing the global Pliocene cooling trend. Concerning northwest Africa, Leroy and Dupont (1994) suggested a gradual increase of the northeast trade winds between 3.3 and 2.5 Ma.

Two different mechanisms for the intensification of the trade winds have been suggested: one ties the strengthening of the atmospheric circulation to the meridional and zonal oceanic temperature gradients; the other links the strengthening of the trade winds to the iNHG. The proposed forcing mechanisms have implications for the timing and variability of the trade wind system during the Pliocene. To test which forcing is more important for the climate of West Africa and the strengthening of the NE trade winds, we investigated vegetation change, pollen transport, and the evolution of the trade wind system for the period of the Late Pliocene to Early Pleistocene (Piacenzian to Gelasian; Cohen et al., 2013) as recorded in the marine sediments retrieved offshore to the west of West Africa.

We present a not-yet-published pollen record of ODP Site 659 in Section 4 comparing it with the pollen record of ODP Site 658 (Leroy and Dupont, 1994) in Section 5. In Section 6 we present new XRF scanning data of ODP Site 659. Using the record of West African vegetation development as well as the dust record of ODP Site 659 (Tiedemann et al., 1994), we interpret the new XRF-scanning results of elemental ratios in ODP Site 659 sediments, which provide a high temporal resolution record of environmental change (Section 7) for two time windows (5.0–4.6 Ma and 3.6–2.5 Ma). Finally, in Section 8 we use the occurrence of pollen grains from northerly (Mediterranean and North-Saharan) sources to discuss when the NE trade winds started to intensify.

2. Modern setting

The modern atmospheric circulation over West Africa has three main components: the northeast trade winds, the African Easterly Jet (AEJ) and the southwest monsoon (Fig. 1). The NE trade winds blow at low altitudes parallel to the African coast. The AEJ blows at

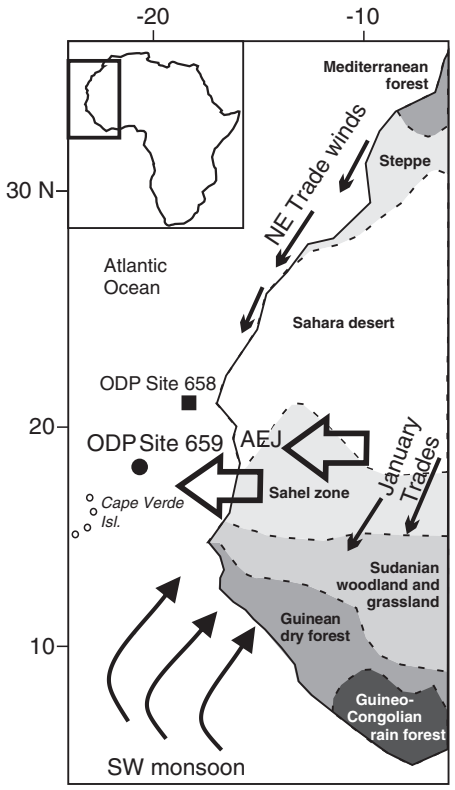

Fig. 1. Modern wind patterns over and vegetation zones in West Africa (Hooghiemstra et al., 2006). Location of ODP Site 659 (this study) and ODP Site 658 (data used for comparison). AEJ: African Easterly Jet.

mid-tropospheric altitudes between 16 and 19°N during most of the year (Nicholson and Grist, 2003). Both wind systems carry mineral dust particles, pollen, spores, diatoms and organic molecules from the continent to the East Atlantic Ocean. The dust coming from the north-western fringe of the Sahara, which is transported by the trade winds is characterised by chlorite, illite (clay fraction) and pale quartz (Sarnthein et al., 1981, 1982). The clay fraction of the dust from the southern Sahara and the Sahel zones, transported by the AEJ, is enriched in kaolinite and abundant reddish-stained quartz that is rich in iron oxides and hydroxides (Sarnthein et al., 1981, 1982; Balsam et al., 1995). The pollen distribution in the marine sediments offshore of North-West Africa depends largely on the wind patterns of the NE trade winds and the AEJ (Hooghiemstra et al., 1986, 2006).

The combined action of the AEJ and the high tropospheric Tropical Easterly Jet (not shown in Fig. 1) is the most important factor influencing the tropical rainbelt, which produces most of the rainfall over the Sahel, effectively independent of the Intertropical Convergence Zone (Nicholson, 2009). The vegetation in northwest Africa strongly depends on the precipitation gradient and is zonally arranged. From north to south the vegetation zones are Mediterranean forest, Steppe, Saharan desert, Sahel zone, Sudanian woodland and grassland, Guinean dry forest and Guineo-Congolian rain forest (White, 1983).

3. Material and methods

Material was sampled from the sediment cores of ODP Site 659 (Ocean Drilling Program, Leg 108) that were retrieved offshore from northwest Africa (18°04 N, 21°01 W), ~530 km from the coast of Mauritania in 1986 (Ruddiman et al., 1987). The site is located on top of the Cape Verde Rise, at 3070 m water depth and bathed by North Atlantic Deep Water (NADW). The sediment cores are composed of

carbonate oozes. The site is considered an open-marine environment site for its very low organic carbon values of less than 0.5% (Stein et al., 1989). We use the age model obtained by Tiedemann et al. (1994) whose stable oxygen isotope curve has been correlated with the benthic stack LR04 published by Lisiecki and Raymo (2005).

116 pollen samples from cores of Hole A of ODP Site 659 were palynologically analysed in 1990 by Suzanne Leroy (38), Lydie Dupont (4), Susanne Jahns (32), and Chiori Agwu (58) and, in 2011, 32 additional samples were analysed from cores 8 to 11, 14 and 15 by Francesca Vallé. Samples of 2 cm thickness (10 and 20 cm^3), were prepared with standard palynological treatment using cold HCl to decalcify followed by cold HF (~40%) attack. The clay and organic fraction smaller than 10–12 μm removed by ultrasonic sieving over an 8 μm mesh. The final residues were stored in water and mounted in glycerol. To calculate concentration values, sample volume was measured by water displacement and one or two tablets containing exotic *Lycopodium* spores were added during the decalcification step.

During resampling in 2011 we discovered that the cores became mouldy in storage, which left fungal hyphens in the samples after palynological preparation. Pollen grains were not visibly degraded. However, in combination with the low pollen concentration the counting of the resampled material turned out to be extremely laborious and time-consuming as hyphens were clogging the slides hiding pollen grains and *Lycopodium* spores. In order to find at least 50 pollen and spores, we analysed up to 10 slides per sample, but never managed to count more than 11% of the original sample (calculated after the counted number of *Lycopodium* spores), whereas in 1990 average counts covered ~20% (and often more than 30%) of the original sample to reach an average of 200 pollen and spores. Pollen percentages are based on the total number of pollen and spores and only calculated if counts exceeded 50 grains. To account for the low counts and the resulting uncertainties we draw confidence intervals ($\alpha = 0.05$) of the relative abundances following the method of Maher (1972). Total pollen and spore accumulation rates were calculated for all samples, using sedimentation rates re-calculated from the age model provided by Tiedemann et al. (1994).

Pollen taxa were identified following the atlas of Bonnefille and Riollet (1980), the African Pollen Database (http://apd.sedoo.fr/pollen/), as well as the reference collection of the Department of Palynology and Climate Dynamics of the University of Göttingen. Pollen of shrubs and trees and other tropical elements have been placed into two groups, Sahel and forest/woodland (see Supplementary Tables 1 and 2), following the same grouping as in ODP Site 658 (Leroy and Dupont, 1994). The interpretation of the pollen record is guided by the modern distribution patterns of pollen and spores in marine sediments offshore from NW Africa (Hooghiemstra et al., 1986, 2006). The palynological results of ODP Site 659 shown in Fig. 2 are compared with those of ODP Site 658 (Supplementary Fig. 1).

XRF scanning has been performed on sediments of ODP Site 659 for a part of the Zanclean (5–4.6 Ma), the Piacenzian (3.6–2.5 Ma), and the last glacial cycle (past 0.14 Ma). We scanned intensities (number of counts per second) of the major light elements Al, Si, Ti, Fe, Ca, K, and Fe directly at the surface of the sediment cores from Hole A and Hole B of ODP Site 659 at 2 cm resolution using the Avaatech XRF core scanner II at the IODP Core Repository at MARUM — Center for Marine Environmental Sciences of the University of Bremen. A detailed description of the instrument and of the measurement techniques can be found in Röhl and Abrams (2000), Richter et al. (2006) and Jansen et al. (1998). Scanning took place in 2011 and 2013. When analysing the data, it became clear that the data scanned in 2013 showed an offset compared to those from 2011. To calculate the offset and to be able to correct for it, we rescanned selected sections and recalculated the intensities to the level of 2011 by linear regression. From the measured and corrected intensities, we calculated the natural logarithm of the elemental ratios Fe/K and Ti/Ca. Using the natural logarithm ensures symmetry of the ratios around zero (Weltje and Tjallingii, 2008; Govin et al., 2012).

We carried out a linear regression analysis between dust percentages and dust accumulation rates (Tiedemann, 1991; Tiedemann et al., 1994) using ordinary least squares and Pearson's r correlation. We calculated 95% confidence intervals of slope and intercept based on direct calculation and bootstrapping (Supplementary Fig. 2). In Section 6 (Tables 1 and 2), we compare the results of pollen analysis and XRF-scanning statistically testing for equal mean (*t*-test), variance (F-test), and median (Mann–Whitney-test). To analyse cyclicity in the elemental ratio record (Section 7), we carried out a continuous wavelet transform of ln(Ti/Ca) and ln(Fe/K) using a Morlet wavelet (wavenumber 6). All statistical analyses were performed with the paleontological statistics package PAST vs 3.0 (Hammer et al., 2001). The significance of the power maxima over red noise has been tested using the module REDFIT (Schulz and Mudelsee, 2002) of the PAST package.

4. Pollen record of ODP Site 659

The pollen diagram of selected taxa is shown in Fig. 2 for the period 3.6 Ma to the present. The sediments of ODP Site 659 are poor in pollen and spores, which generally are well preserved. The pollen and spore accumulation rates fluctuate between 0 and 2000 grains per cm^2 per thousand years ($N/cm^2/ka$) showing low values in the upper and lowermost parts of the record and high and variable ones in between. Accumulation rates of the summed pollen of *Pinus*, *Ephedra*, and *Artemisia* (TW, trade wind indicators) increase first during the Gelasian and reach maximum values in the Middle Pleistocene.

The most abundant pollen taxon is Poaceae with an average value of ~30%. Other abundant pollen taxa are Caryophyllaceae and Amaranthaceae including Chenopodiaceae (=CA), Cyperaceae, Asteraceae (Liguliflorae, Tubuliflorae, and *Artemisia* pollen types), and *Ephedra* (Fig. 2). Sparsely occurring pollen taxa have been lumped into two groups, forest elements from the Sudanian and Guinean vegetation (95 taxa, Supplementary Table 1) and pollen from Sahelian taxa (25 taxa, Supplementary Table 2). Fern spores do not exceed 20% (of the total pollen and spores) and are mainly found in the older part of the record (before 1.5 Ma) parallel to raised percentages of *Rhizophora* pollen (Supplementary Fig. 1). Moderate fern spore percentage maxima (10–20%) occur around 2.85 Ma, between 2.2 and 2.6 Ma, and around 0.95 Ma, when the representation of forest/woodland is high.

The relative abundance of Poaceae pollen is high until 2.6 Ma and gradually declines thereafter (Fig. 2). Another maximum occurs shortly before 2 Ma. After 1.5 Ma grass pollen percentages are rather stable with an average of just over 20%. Pollen abundance from the Sahel and forest/woodland is also higher prior to 1.5 Ma and declines to very low values after 0.9 Ma. The second most abundant pollen taxon is CA reaching values exceeding 50% between 2.8 and 1.4 Ma. *Artemisia* and *Ephedra* pollen percentages are high (~20%) after 0.5 Ma; other *Ephedra* pollen percentage maxima occur between 2.2 and 1.9 Ma, when *Artemisia* pollen percentages are low. Shortly before 2.5 Ma, a maximum occurs for both *Ephedra* and *Artemisia*.

The Asteraceae record shows some remarkable maxima before 3 Ma, while values for Liguliflorae and Tubuliflorae are rather low throughout the rest of the Pliocene and in the Pleistocene (Fig. 2). An isolated Tubuliflorae pollen percentage maximum occurs at 1.3 Ma, but the temporal resolution of the record for this period is too coarse to draw conclusions from it. Besides low Cyperaceae pollen percentages during the past 300 ka, no trend can be found for the rest of the Cyperaceae record. Maximal values between 30 and 40% occur in both Pliocene and Pleistocene.

5. Pliocene and Pleistocene trends in West African vegetation

Before we present the results of XRF scanning we compare the pollen records of ODP Sites 659 and 658 (Leroy and Dupont, 1994) to obtain a robust interpretation of the palynological results of ODP Site

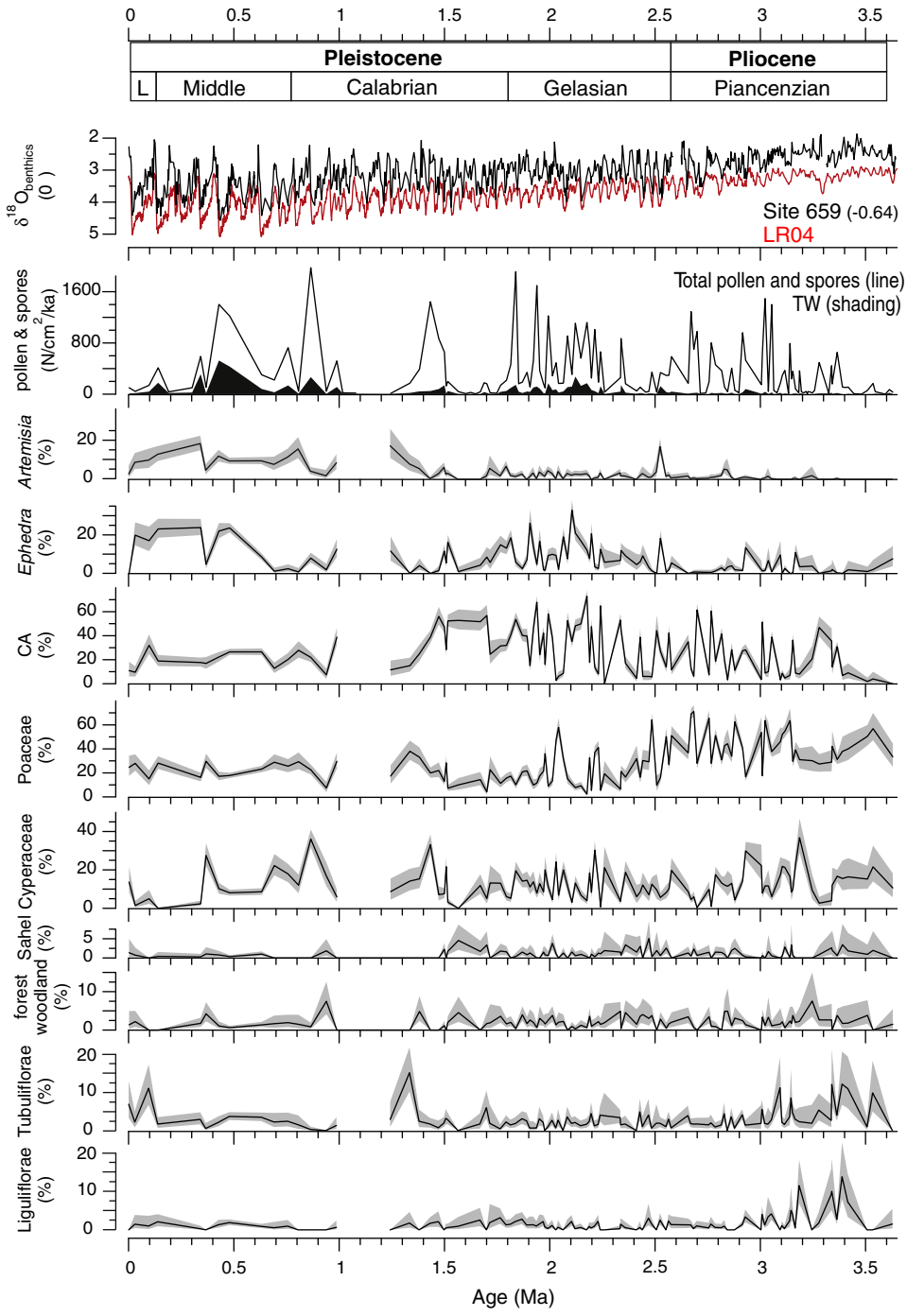

Fig. 2. Pollen record of ODP Site 659. From top to bottom; chronostratigraphy version 2014/02 (Cohen et al., 2013); stable oxygen isotope stratigraphy of ODP Site 659 (upper, Tiedemann et al., 1994; $\delta^{18}O$ values of Site 659 are plotted 0.64 per mil below seawater equilibrium) compared to the global stack LR04 (lower, Lisiecki and Raymo, 2005). Total pollen and spore accumulation rates (line); accumulation rates of trade wind transported pollen (TW; shaded black); pollen percentages of selected taxa (*Artemisia*, *Ephedra*, CA = Caryophyllaceae and Amaranthaceae, Poaceae, Cyperaceae), groups (Sahel, forest/woodland), Tubuliflorae (not including *Artemisia*), and Liguliflorae. Age model after Tiedemann et al. (1994). 95% confidence intervals of the percentage data are indicated by grey shading.

659. Age models (Tiedemann, 1991; Tiedemann et al., 1994; Leroy and Dupont, 1997) and the correlation between both sites rely on the stable oxygen isotopes of benthic foraminifera (*Cibicidoides wuellerstorfi*) (Supplementary Fig. 1). The pollen records of the two sites overlap between 3.7 and 1.7 Ma and between 0.8 and 0 Ma covering the Piacenzian, the Gelasian, and the Middle and Late Pleistocene (Brunhes Chron). The record of Site 659 has a lower temporal resolution and lower pollen counts resulting in relatively large error bars (given as 95% confidence intervals). The great distance of Site 659 to the coast (530 km), being almost three times as far offshore as Site 658 (200 km), results in 10 times lower pollen concentrations. Moreover, sedimentation rates at Site 659 vary between 1 and 6 cm/ka and those of Site 658 range between 5 and 40 cm/ka, mostly exceeding 10 cm/ka. Despite large differences in the distance to the coast and the sedimentation rates between Sites 658 and 659, their pollen records are remarkably similar in composition and relative abundance (percentages).

Within the Asteraceae three pollen taxa have been distinguished: *Artemisia*, Liguliflorae (Tribus Lactuceae after Bremer, 1994), and

Table 1
Testing differences in total pollen accumulation rates (PAR) and percentages of grass (Poaceae) and Caryophyllaceae–Amaranthaceae (CA) between samples showing Ti/Ca maxima or minima indicating relatively dusty or non-dusty conditions, respectively. C.I., confidence interval; MW-test, Mann–Whitney test.

Pollen	Poaceae %		Ca %		Par per cm^2 per ka	
	Dusty	Non-dusty	Dusty	Non-dusty	Dusty	Non-dusty
Number	18	24	18	24	18	45
Mean	33.47	47.44	30.88	13.34	521.94	188.64
95% C.I.	28.74	40.74	21.91	8.44	352.69	92.32
	38.20	54.15	39.85	18.23	691.19	284.97
Variance	90.60	252.11	325.38	134.33	115830	102800
Median	31.13	50.37	29.57	9.55	452.79	56.22
F-test	$P < 0.05$		$P < 0.05$		$P > 0.05$	
T-test	($P \ll 0.01$)		($P \ll 0.01$)		$P \ll 0.01$	
MW-test	$P \ll 0.01$		$P \ll 0.01$		$P \ll 0.01$	

Tubuliflorae (the rest except for *Artemisia*). *Artemisia* pollen is mainly trade wind transported as the plants grow in the Mediterranean region and the transitional steppes between the Mediterranean and Saharan vegetation (White, 1983; Hooghiemstra et al., 1986). *Artemisia* pollen percentages show the same pattern of stepwise increasing values since the late Pliocene at both cores, i.e. an early maximum at 2.53 Ma and increased values during the past 0.5 Ma (Supplementary Fig. 1).

The record for other Asteraceae pollen is remarkably different. Tubuliflorae and Liguliflorae percentage maxima are found in the Piacenzian, before 3 Ma, but the percentages remain low for the rest of the record at both ODP sites (Supplementary Fig. 1; Fig. 6). The Liguliflorae pollen grains mainly originate from species of the Tribus Cichorieae (=Lactuceae, Bremer, 1994), which nowadays are scarce in tropical West Africa (Hutchinson and Dalziel, 1963) as indicated by low pollen percentages (<10%) in modern marine sediments offshore from West Africa south of 27°N (Hooghiemstra et al., 1986). Pollen percentages of Asteraceae from modern terrestrial surface sediments are low in the central and southern Sahara and Sahel and higher Asteraceae percentages in the Sudanian savannah region of Nigeria are attributed to modern anthropogenic pressure (Lézine, 1987; Schulz, 1991). Leroy and Dupont (1994) proposed that the Liguliflorae pollen during this period would originate from savannah species and that no modern analogue for this type of savannah exists anymore. The record of ODP Site 659 also reveals increased representation of Asteraceae before 3 Ma corroborating the earlier inferences from ODP Site 658.

The group of woodland/forest comprises 95 pollen taxa whose source areas are mainly in the Sudanian woodland and grassland and Guinean dry forest (Supplementary Table 1) and together make up less than 8% of the pollen assemblage. Most tropical trees produce little pollen, which is not well dispersed by wind (Dupont and Agwu, 1991). The pollen percentages for forest and woodland are slightly higher at ODP Site 659 (Supplementary Fig. 1), which is explained by its location being almost three degrees of latitude south from ODP Site 658. Percentages are somewhat higher in the Pliocene than in the Pleistocene, whose trend is similar for both cores. The Sahel group comprises 25 pollen taxa from the grassland, wooded grassland, and shrubland of the Sahel (Supplementary Table 2). Grass (Poaceae) pollen originates mainly from the Sahel and the Sudanian savannah as indicated by the modern pollen distribution in marine surface sediment samples (Hooghiemstra et al., 1986). Most maxima in the Sahel pollen co-occur with maxima in the grass pollen percentages emphasising that both groups have their main sources in the same biomes. The higher temporal resolution of the Site 658 record (Supplementary Fig. 1) reveals strong fluctuations in the grass pollen percentages, but the trends are the same in ODP Sites 659 and 658. Again the representation of grasses and Sahelian taxa is higher in the Pliocene and declines after 2.5 Ma. Between 2.3 and 1.8 Ma grass pollen percentages fluctuate strongly at Site 658, but at Site 659 only two maxima are recorded. At both sites, values are relatively low during the past 0.3 Ma.

Table 2
Testing differences in total pollen accumulation rates (PAR) and percentages of grass (Poaceae) and Caryophyllaceae–Amaranthaceae (CA) between samples showing Fe/K maxima or minima indicating relatively wet or dry conditions, respectively. C.I., confidence interval; MW-test, Mann–Whitney test.

Pollen	Poaceae %		Ca %		Par per cm^2 per ka	
	Dry	Wet	Dry	Wet	Dry	Wet
Number	17	23	17	23	17	23
Mean	30.80	51.23	30.28	12.21	473.63	383.02
95% C.I.	26.01	46.45	19.99	8.80	293.07	206.31
	35.59	56.00	40.56	15.62	654.19	559.73
Variance	86.64	121.89	400.35	15.62	654.19	559.73
Median	30.86	51.02	30.80	10.00	406.93	191.12
F-test	$P > 0.05$		$P < 0.01$		$P > 0.05$	
T-test	$P \ll 0.01$		($P \ll 0.01$)		$P > 0.05$	
MW-test	$P \ll 0.01$		$P < 0.05$		$P > 0.05$	

The woody shrubs *Calligonum* and *Ephedra* presently grow in the northern Sahara and the transitional steppes between the desert and the Mediterranean vegetation (Knapp, 1973; White, 1983). Their pollen distribution in modern marine sediments reaches south of the latitudinal plant distribution as the result of pollen transport by the trade winds (Hooghiemstra et al., 1986). At both ODP Sites 658 and 659 *Calligonum* pollen percentages increased from 2.5 to 2.2 Ma and during the last Glacial (Supplementary Fig. 1). At Site 659 *Ephedra* pollen percentages had already increased to values over 20% at the beginning of the Pleistocene (maxima around 2.1 and around 1.9 Ma), while at Site 658 such values are reached only in the past 0.5 Ma. The higher relative abundance of *Ephedra* pollen at the southern site might indicate an increase of *Ephedra* in the Sahara south of 21°N (latitude of ODP Site 658) during the Gelasian.

During the Gelasian the representation of CA is high. Sources of CA pollen are mainly along the coast and in the Sahara and many Amaranthaceae species grow on saline soils. Their pollen is distributed westwards by the easterly flow of the AEJ (Hooghiemstra et al., 1986). An increase in desert vegetation since 2.7 Ma is indicated by recurrent maxima in CA pollen percentages at ODP Sites 659 and 658 (Supplementary Fig. 1). For the period between 2.3 and 1.7 Ma, the Site 658 record shows high variability with rapidly repeating maxima. During the Middle and Late Pleistocene the CA pollen percentages are generally lower at ODP Site 659 than at Site 658.

TW pollen sums up the counts of *Artemisia*, *Ephedra*, and *Pinus* pollen. The transport of these pollen types to ODP Sites 658 and 659 is almost exclusively by the NE trade winds (Hooghiemstra et al., 1987). Our TW group deviates from the original trade wind indicators as described by Hooghiemstra et al. (1987) and Hooghiemstra (1988) leaving out the Asteraceae other than *Artemisia*. TW pollen concentrations at Site 658 are ten times higher than at Site 659, but fluctuations and trends in the TW record run parallel at both sites (Supplementary Fig. 1; Fig. 6). Shortly before 2.5 Ma, maxima in the TW pollen concentration concurrent in both sites mark the intensification of NE trade winds at the start of the Pleistocene. Leroy and Dupont (1994) inferred earlier short periods with increased trade wind vigour, but while comparing the pollen records of ODP Site 659 and 658, we argue that the main trade wind intensification occurred during the Pliocene–Pleistocene transition. During this period, relative abundance maxima of *Artemisia* and *Ephedra* pollen are recorded at both sites and a *Pinus* pollen percentage maximum is found at ODP Site 659. Increased pollen percentages of *Artemisia*, *Ephedra*, and *Pinus* occurred intermittently between 3.7 and 2.7 Ma, but concentrations are low.

In summary, the new record of ODP Site 659 confirms the results of ODP Site 658 which have been previously interpreted as a record of the existence of a no analogue Asteraceae-rich (notably Cichorieae) savannah between 3.6 and 3.0 Ma in West Africa (Leroy and Dupont, 1994). Between 3.0 and 2.5 Ma the savannah changed in composition and periods with extended desert vegetation became more and more frequent.

After 2.6 Ma, woodland and forest declined, trade winds became important, and desert vegetation further extended. Increasing the temporal resolution of our record might reveal the mechanism leading to vegetation and climate shifts associated with the intensification of the Northern Hemisphere glaciations at 2.6 Ma. Therefore, we XRF scanned sediments dated between 3.6 and 2.5 Ma (Piacenzian), between 5.0 and 4.6 (part of the Zanclean) and of the past 0.14 Ma (last glacial cycle) at an average resolution of 0.5 to 1.2 ka.

6. XRF scanning; results and interpretation

The major element intensities (counts per second) differentiate between terrestrial and marine origins of the elements (Fig. 3). The counts of terrigenous elements aluminium (Al), titanium (Ti), potassium (K), silicon (Si), and iron (Fe) fluctuate consistently but opposite to those of the element calcium (Ca) that is almost an order of magnitude more abundant than the most abundant terrigenous element, Fe. Intensities of all terrigenous elements including Si correlate with the dust percentage record of Tiedemann (1991). The maximum in the terrestrial elements, however, has been counted in a dark layer of sediment, dated at 3.07 Ma and recognised by Faugères et al. (1989) as one of the few turbidites reaching the Cape Verde Rise during this part of the Pliocene (marked as "T" in Fig. 3). Subsequently, we discarded the turbidite samples from further analysis.

The elemental composition of dust reflects its mineralogical composition (Scheuvens et al., 2013) depending in turn on the soil types and on the climate conditions in which the soils are formed, while the mineralogy of the dust holds information about the source area (Moreno et al., 2006; Govin et al., 2012). In this study we present the variations of Fe/K and Ti/Ca ratios (Fig. 4). As the Al counts are very low, probably because of the site's great distance from the shore, we cannot use the Al/Si ratio as an indicator of dust supply (Collins et al., 2013).

To interpret the changes in the ratios, we look at the implied sources of the terrigenous elements. Most of the Ca contained in the Atlantic surface sediments can be assigned to carbonates of marine origin (e.g. Jansen et al., 1998; Arz et al., 1999; Govin et al., 2012). Si is the most abundant element in mineral dust and mainly incorporated in quartz grains (Scheuvens et al., 2013). It could also be related to biogenic opal; however, opal concentration in ODP Site 659 sediments is lower than 2% and considered negligible (Tiedemann et al., 1989). Today, dust coming from the north-western fringe of the Sahara is enriched in pale quartz, illite and feldspar (Sarnthein et al., 1981) and dust coming from the southern Sahara and Sahel zone is rich in Fe-stained quartz and kaolinite (Sarnthein et al., 1981). Ti represents an important crustal indicator and high Ti contents in aerosol samples are proposed as a marker for Saharan dust (e.g. Nicolás et al., 2008), which is often enriched in Ti. For example the source sediments of the Bodélé depression (central Sahara) exhibit high Ti/Al ratios (Scheuvens et al., 2013).

Possible sources of Fe are iron oxides and hydroxides (hematite and goethite) that are a component of the distal aeolian dust, while quartz grains represent coarser grain size (Balsam et al., 1995). K is associated with many aluminosilicates such as illite (Scheuvens et al., 2013) or potassium feldspar (Zabel et al., 2001) that are abundant in soils with reduced chemical weathering (Govin et al., 2012). Modern dust filter contents show that the Fe/K ratio is twice as high in dust from the savannah as from the Sahel because of the deep chemical weathering of tropical soils (Mulitza et al., 2008).

To test whether the Ti/Ca ratios can be used as a dust proxy at ODP Site 659, we compared those ratios to the dust content calculated from the carbonate free siliciclastic content, which can be regarded as the terrestrial component because the Plio-Pleistocene sediments of ODP Site 659 hardly contain biogenic opal or volcanic glass (Tiedemann, 1991). The ln(Ti/Ca) is linearly correlated to the dust percentages ($r^2 = 0.82$; Supplementary Fig. 2) as also observed for the last glacial cycle from ODP Site 659 (Kuechler et al., 2013). A lesser though still significant correlation ($r^2 = 0.54$) exists between the ln(Ti/Ca) and the accumulation rates of dust; but we prefer the correlation between ln(Ti/Ca) and dust percentage as both measures concern relative abundance. The correlation is good enough to consider the ln(Ti/Ca) a proxy for dust percentages in sediments of ODP Site 659, whereby

$$\ln(\mathrm{Ti/Ca}) = 0.05 \times \mathrm{dust}\% - 6.9. \quad (1)$$

Some Ti/Ca ratios are particularly low during the Zanclean (Fig. 4) and the residuals from the regression display negative values (Supplementary Fig. 2). Obviously the linearity of the relationship between ln(Ti/Ca) and dust percentages breaks down at very low values of dust. When dust is scarce the dust percentages either overestimate or the ln(Ti/Ca) values underestimate the dust supply. During the last glacial cycle, the residuals are positive; here the Ti/Ca ratios are generally high while the dust percentages strongly fluctuate.

For further characterisation, we compare Fe/K and Ti/Ca ratios of specific samples with their pollen content (Fig. 4). Our rationale is that while dusty periods are recorded by high Ti/Ca ratios, humid periods would be recorded by high Fe/K ratios. We put pollen samples into four different groups depending on maxima and minima in the Fe/K and Ti/Ca ratios and tested differences in total pollen accumulation rates and pollen percentages of Poaceae and CA between dusty samples (Ti/Ca maxima) and non-dusty ones (Ti/Ca minima) and between samples from wet periods (Fe/K maxima) and arid ones (Fe/K minima). The results are presented in Tables 1 (dusty vs non-dusty) and 2 (wet vs arid).

The F-test indicates that the variance for Poaceae and CA pollen percentages differs between the dusty and non-dusty groups, but the dusty and non-dusty pollen accumulation rates have about the same variance. Thus, only the result of the *t*-test in the accumulation rates is robust. The Mann–Whitney test, however, indicates that the medians differ significantly. Pollen accumulation rates and CA pollen percentages are higher and Poaceae pollen percentages are lower when terrestrial dust is abundant as indicated by the Ti/Ca ratio. It seems that concerning total pollen accumulation at ODP Site 659, wind transport is the most important. Pollen accumulation rates have previously been used as an indicator of the transport capacity of the wind systems (Hooghiemstra, 1988; Hooghiemstra et al., 2006).

Concerning the difference between samples from humid (high Fe/K) and arid (low Fe/K) periods (Table 2), the F-test indicates that the variance in the groups for Poaceae pollen percentages and accumulation rates is about the same, but the CA pollen percentages differ in variance. Thus the *t*-test result is not robust for the CA percentages. Accumulation rates do not differ significantly between wet and dry periods, but Poaceae percentages are higher and CA percentages are lower during wet periods as indicated by the Fe/K ratio.

We interpret these results as follows: during dusty periods more pollen is transported to the site by easterly and north-easterly winds; during wetter periods savannah grassland extended as indicated by the high Poaceae pollen percentages; during drier periods desert vegetation extended as indicated by the high CA pollen percentages. However, the pollen accumulation rates do not allow distinction between humid and arid periods, which is possibly the result of the opposing effects of increased terrestrial input and less pollen producing vegetation during arid periods.

7. Environmental change in West Africa prior to the iNHG

With the results of the previous section in mind, we interpret the high resolution ln(Ti/Ca) and ln(Fe/K) record of the Piacenzian and part of the Zanclean, in which we did not find enough pollen for analysis. A continuous wavelet transform traces the development in the pacing of climatic fluctuations (Fig. 5). We interpolated the data to equidistant steps of 1 ka for the period from 4.99 to 4.60 Ma and from 3.62 to 2.53 Ma. We used the age model of Tiedemann et al. (1994). Application

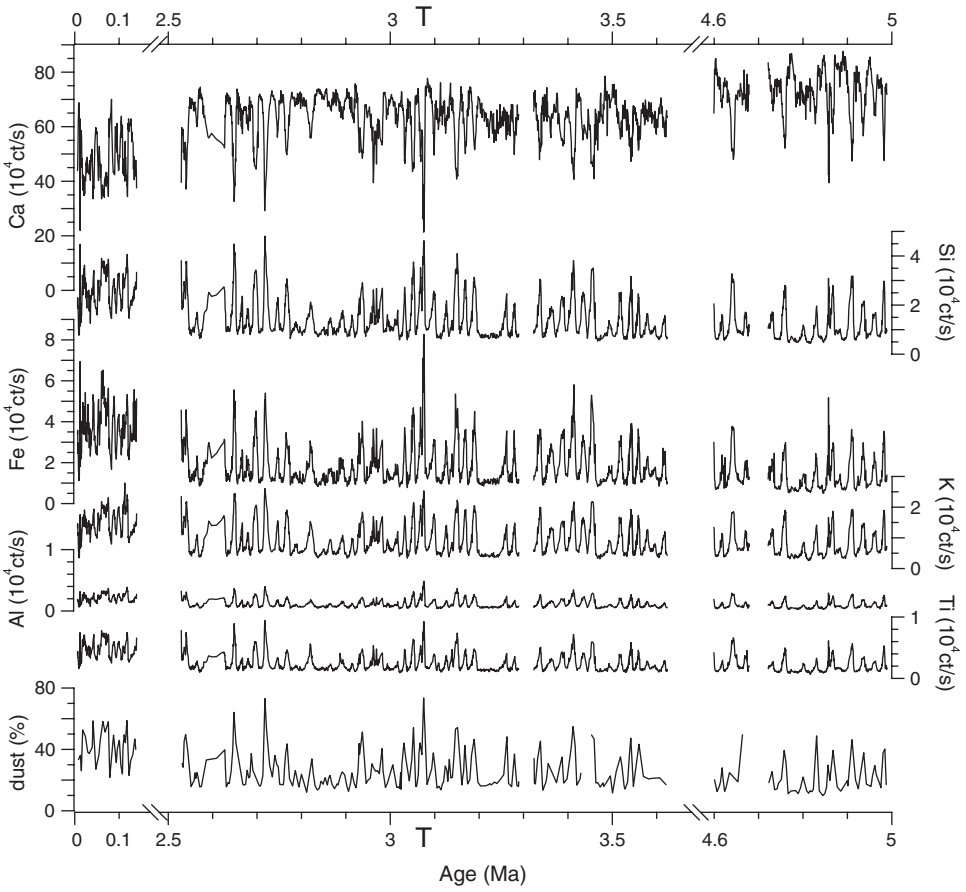

Fig. 3. Major element intensities (counts per seconds) of calcium (Ca), silica (Si), iron (Fe), potassium (K), aluminium (Al), and titanium (Ti) compared with dust percentages of ODP Site 659 (Tiedemann, 1991; Tiedemann et al., 1994) for the intervals 5.0 to 4.6 Ma, 3.62 to 2.54 Ma, and 0.14 to 0 Ma. T indicates a turbidite that is discarded from further analysis.

of the alternative model of Clemens (1999), which shifts most ages older than 3 Ma by roughly one precession cycle (maximum 28 ka), leads to very similar results.

Not surprisingly, variability and trends in the ln(Ti/Ca) record is similar to those inferred by Tiedemann et al. (1994) from the dust accumulation rates. The amount of dust is slightly less during the Zanclean part (5.0–4.6 Ma) than during the Piacenzian (3.6–2.6 Ma) and the dust is much less in the Pliocene compared to the last glacial cycle. The number of dust outbreaks was less during the Zanclean and increased in the Piacenzian. The power at the precession band (19–23 ka) varies between 3.6 and 2.5 Ma; power at the obliquity band (41 ka) is relatively low between 3.4 and 3.0 Ma; power at the 100 ka band shows maximum values between 4.8 and 4.6 Ma and between 3.3 and 2.9 Ma (Fig. 5).

The variability and frequencies in the Fe/K ratios differ strongly from those in the Ti/Ca ratios. Fe/K ratios, indicating changes in humidity, have more high-frequency variability (significant periodicities between 2 and 3 ka) than the Ti/Ca ratios, especially during the Zanclean. This result underlines that dust is not a good indicator for aridity as its production additionally depends on the lack of vegetation and on ephemeral fluvial activity (Trauth et al., 2009). Interesting is the suborbital variability in the Fe/K ratios existing long before the iNHG suggesting that millennial cycles in tropical climate may be forced, at least in part, by processes independent from high latitude icecaps (Peterson et al., 2000). On the other hand, after 2.9 Ma power in the precession band increased indicating a role of the growing Northern Hemisphere ice-sheets on the pacing of tropical humidity cycles in West Africa.

Although the short-term fluctuations in the Fe/K ratios generally agree with the pollen interpretation (see previous section), the long-term trends do not. While pollen records indicate more desert and more arid conditions during the last glacial cycle compared to the Pliocene, the average Fe/K ratios are higher in the last glacial cycle (Fig. 4). The average ln(Fe/K) value rose from 0.57 in the Zanclean to 0.78 in the Piacenzian before 3 Ma. It dropped slightly during the Piacenzian from 0.78 between 3.6 and 3.0 Ma to 0.71 between 3.0 and 2.5 Ma, but is much higher, 0.92, in the last glacial cycle. Similarly, the average dust content during the last glacial cycle is significantly higher (41%) than during the Pliocene (21% in the Zanclean and 26% in the Piacenzian). Interpreting the Fe/K long-term trend as an indication of generally increasing humidity in West Africa since the beginning of the Pliocene would be at odds with other terrestrial and marine records (e.g. Ruddiman et al., 1989; Dupont and Leroy, 1995; deMenocal, 2004; Salzmann et al., 2008) and contrary to the accepted view that Fe/K ratios become higher under wetter conditions because of the effect of weathering (Zabel et al., 2001). A more likely explanation for the rising trend in Fe/K ratios is a slow and gradual change in the source area, maybe a shift southwards as vegetation belts moved south, from less weathered soils to deeply weathered ones that are richer in iron (Fe) and/or more depleted in potassium (K).

In Fig. 6, the Ti/Ca and Fe/K ratios are compared with SST and plant wax records from IODP Site U1313 (Leg 306) in the central North Atlantic (Naafs et al., 2010, 2012). The most prolonged humid period in West Africa based on the Fe/K ratios occurred between 3.24 and 3.20 Ma. At that time temperatures in the North

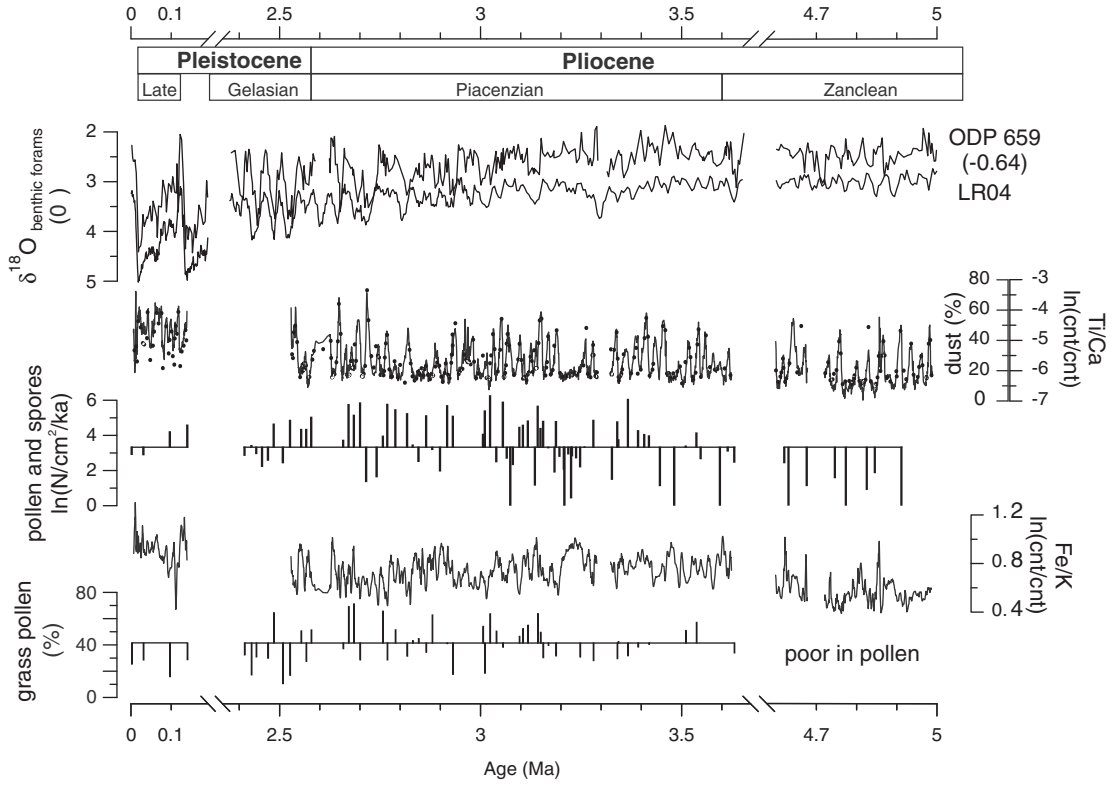

Fig. 4. Comparing XRF scanning and pollen results. Chronostratigraphy version 2014/02 (Cohen et al., 2013). Stable oxygen isotopes of ODP Site 659 (Tiedemann et al., 1994) compared to the global stack LR04 (Lisiecki and Raymo, 2005). $\delta^{18}O$ values of Site 659 are plotted 0.64 per mil below seawater equilibrium. Ti/Ca ratios (line) and dust percentages (dots) of ODP Site 659 compared with the accumulation rates of total pollen and spores (bars upward and downward the mean of 3.3). Fe/K ratios (5 point moving average) compared with grass (Poaceae) pollen percentages (bars upward and downward the mean of 41). Total pollen accumulation varies with the Ti/Ca ratios (Table 1) and the dust input. Samples characterised by high Fe/K ratios mostly have more than average grass pollen percentages (Table 2).

Atlantic at 41°N were between 22 and 20 °C (Naafs et al., 2010). During this period the terrestrial input at ODP Site 659 was very low, thus precluding a pollen record. Also the aeolian input of terrestrial material from North America in the North Atlantic was minimal during this period (Naafs et al., 2012). Fortunately, ODP Site 658 – situated much nearer to the coast – does have a pollen record revealing a strong increase in the representation of woody elements of the Sudanian and Guinean vegetation (Fig. 6) and low values for elements from the desert such as *Ephedra* and CA.

The period between 3.24 and 3.20 Ma is the wettest and most stable period in West Africa during the Piacenzian. Expansion of steppe and wooded grasslands during this period is reported by Bonnefille et al. (2004) for eastern Africa at the Hadar section, also suggesting wetter conditions compared to present-day arid conditions. Our data support previous modelling studies of the mid-Pliocene (mid-Piacenzian) warm period (~3.3–3.0 Ma), which reconstructed increased precipitation in subtropical Africa (Contoux et al., 2012) and indicate a smaller Sahara desert and a northward expanded woodland vegetation into today's arid region (Salzmann et al., 2008). These warmer and wetter conditions probably were similar to the ones reconstructed for the Holocene African Humid Period, between ca. 14.8 and 5.5 ka (deMenocal et al., 2000a), when the Sahara desert was covered with grasses and shrubs (COHMAP Members, 1988), palaeolakes were extended (Gasse, 2000), and the dust supply to the eastern Atlantic was drastically reduced (deMenocal et al., 2000b). In both cases (Holocene and Pliocene), eccentricity and with it the precession variability in insolation was low, but atmospheric CO_2 might have been higher during the Pliocene (Laskar et al., 1993; Bartoli et al., 2011).

8. The onset of strong NE trade winds over Africa

Based on meridional SST differences in the equatorial Pacific (e.g. Lawrence et al., 2006), several authors suggest that enhancement of the zonal and meridional atmospheric circulation, including the trade winds, already started around 3 Ma (Wara et al., 2005; Fedorov et al., 2006). Others, however, date the strongest increase of the zonal temperature gradient much later, i.e. at 2.2–2.0 Ma (Etourneau et al., 2010; Steph et al., 2010). Concerning the latter scenario, a positive feedback cycle was possibly established around 2 Ma, in which decreasing SSTs, intensified trade winds and increased wind-driven upwelling favoured long-term sequestration of atmospheric carbon dioxide in the sediment (Marlow et al., 2000).

In both cases, the strength of the trade winds is associated with the meridional SST gradient. To investigate whether the dust supply from West Africa is related to the meridional SST gradient, we compared our Ti/Ca dust record with several SST records from the Atlantic, ODP Sites 662, 607, 982 (Lawrence et al., 2009, 2010; Herbert et al., 2010), and with the SST differences between the Equatorial Atlantic Site 662 and the North Atlantic Site 607 (Fedorov et al., 2013). We did the same with our Fe/K record to test the relationship between Atlantic SSTs and SST gradients with West African humidity between 3.5 and 2.5 Ma (not shown). We could not find any consistent correlation between the SST and our records, at least not for the period before 2.7 Ma. If there is a relationship between dust and aridity in West Africa and SST of the North Atlantic, it is not a simple one.

The upwelling history offshore from Mauretania might reveal the timing of the beginning of strong NE trade winds. Grain size distribution

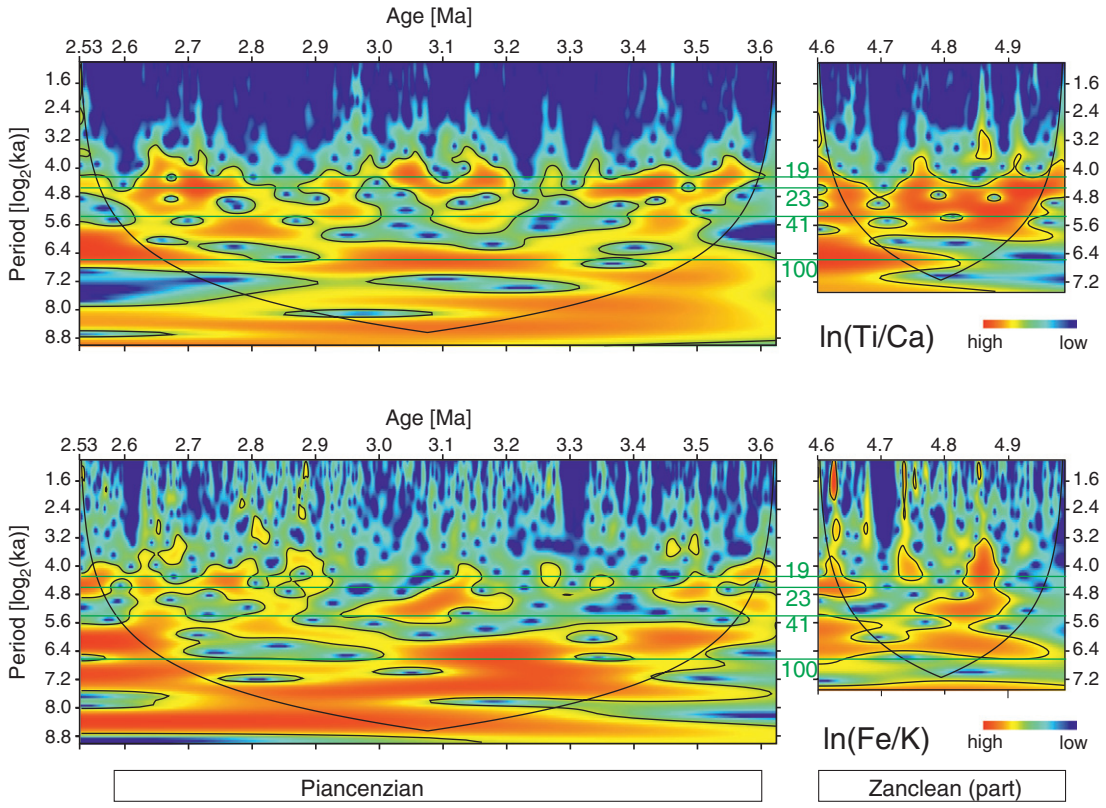

Fig. 5. Continuous wavelet transform (Morlet 6) of ln(Ti/Ca) (top) and ln(Fe/K) (bottom) of ODP Site 659 for the Pliocene periods between 2.53–3.62 Ma (left) and 4.60–4.99 Ma (right). Data are linearly interpolated to 1 ka steps using the age model of Tiedemann et al. (1994). On the X-axis age in Ma; on the Y-axis periodicities in ka on a $\log_2$-scale. Orbital periodicities are indicated by green lines. Signal power (squared correlation strength with the scaled mother wavelet) is in colour. Black contours give the significance level corresponding to $p = 0.05$ after a chi-squared test with the null hypothesis of a white noise model (Torrence and Compo, 1998). Cone of influence (black line) indicates the region of boundary effects.

of ODP Site 658 indicates that regular river input of fluvial clays occurred prior to 3.0 Ma, which reduced stepwise between 3.0 and 2.5 Ma during glacial periods (Tiedemann et al., 1989). An early maximum of the biogenic opal at ODP Site 658 would indicate that coastal upwelling offshore from Cape Blanc began around 3 Ma suggesting an increase of the northeast trade winds by that time (Tiedemann et al., 1989). However, the three main opal maxima at ODP Site 658 fall in "warm" periods (minima in the oxygen isotope stratigraphy) and could also have been induced by river-borne nutrients instead of upwelling. Moreover, Etourneau et al. (2012) argue that upwelling globally was weak between 3 and 2.7 Ma and that in the case of the Benguela upwelling system high diatom and opal productivity in the South Atlantic occurred under weak upwelling, even stratified, conditions.

The NE trade wind history probably is better recorded in the concentrations of TW pollen (Fig. 6). Comparison of the pollen records of ODP Sites 659 and 658 shows the first concurrent maximum in TW pollen concentration occurring at 2.53 Ma. TW pollen concentrations remain at a higher level afterwards. The TW maximum shortly before 2.5 Ma is preceded by two maxima recorded at Site 658 only (~2.7 and 2.6 Ma). Earlier maxima of trade wind indicators are rather ambiguous. Prior to the 2.7 Ma, before the iNHG, little or no systematic relationship occurs between SST of the North Atlantic with aridity and dust in West Africa (Fig. 6). This changes around 2.7 Ma (Marine Isotope Stage G6/G4), when, in the central North Atlantic (IODP Site U1313), the first maximum in aeolian input of *n*-alkanes (higher plant waxes) is registered together with a minimum in SST (Naafs et al., 2010, 2012). Naafs et al. (2012) attribute the aeolian higher plant wax supply to sources made accessible by glacial erosion and transported by westerly winds from North America. The next combined SST minima and wax maxima at Site U1313 occurred at 2.6 (Marine Isotope Stage 104) and just before 2.5 Ma (Marine Isotope Stage 100). During the glacial period of Stage G6/G4 and the two sequels around 2.6 and 2.5 Ma, aridity (decreasing Fe/K ratios) and dust levels (increasing Ti/Ca ratios) in West Africa correlate with the indication of increased NE trade winds (TW pollen concentration at Site 658). These results associate the increase of trade wind strength in West Africa to the intensification of the Northern Hemisphere glaciations.

9. Conclusions

Terrestrial input to the marine sediments of ODP Site 659 is almost exclusively aeolian. The ratio between titanium and calcium expressed as ln(Ti/Ca) can serve as a proxy for dust input at the site. Pollen transport by easterly and north-easterly winds increased during dusty periods.

Savannah grassland expanded during wetter periods characterised by high ln(Fe/K) values and desert vegetation expanded during drier periods characterised by low ln(Fe/K) values.

During the Pliocene, humid climate alternates with arid and dusty conditions in West Africa. The longest period of warm and humid climate occurred between 3.24 and 3.20 Ma, which only covers a part – albeit the warmest one – of the mid-Pliocene (mid-Piacenzian) warm period.

Comparison of the pollen records of ODP Sites 659 and 658 revealed remarkable similarities in composition adding confidence to the reconstruction of vegetation change in Pliocene West Africa. Shifts of the vegetation between woodlands, grasslands and desert occurred at

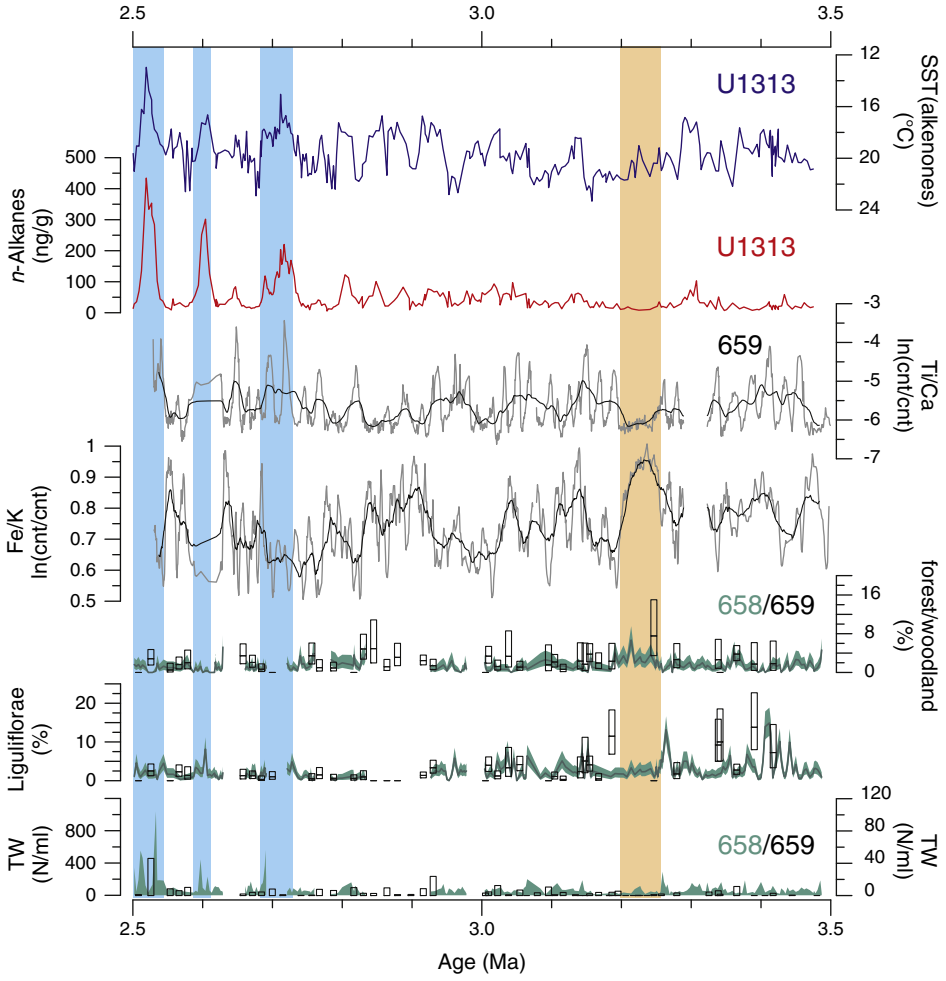

Fig. 6. Comparison of Ti/Ca (thin grey line ln(Ti/Ca); thick black line ln(Ti/Ca) 31-point moving average) and Fe/K ratios (thin grey line ln(Fe/K) 5-point moving average; thick black line ln(Fe/K) 31-point moving average) of ODP Site 659 with alkenone derived SSTs (Naafs et al., 2010) and *n*-alkane concentration (Naafs et al., 2012) of ODP Site 306-U1313 in the North Atlantic (41°N 33°W). Note the reversed scale of the alkenone SST. Pollen percentages of forest/woodland elements and of Asteraceae Liguliflorae from ODP Sites 658 (line and shading) and 659 (boxes). 95% confidence intervals are denoted by the width of the shading (Site 658) and the length of the boxes (Site 659). TW pollen concentration as an indication of NE trade wind vigour at ODP Sites 658 (shading) and 659 (boxes). Humid conditions prevailed between 3.24 and 3.20 Ma (reddish bar). Strengthening of the NE trade winds was concurrent with increased supply of plant wax (*n*-alkanes) to the North Atlantic during the intensification of the Northern Hemisphere Glaciations (blue bars) around 2.7, 2.6, and just before.

orbital time scales. The long-term trend reveals a decline of woodland and forest after 2.6 Ma. The desert extended substantially since 2.7 Ma.

The high relative abundance of Asteraceae Liguliflorae pollen indicates that species from the Tribus Cichorieae (=Lactuceae after Bremer, 1994) might have grown in the savannah until 3 Ma. The floristic composition changed and the savannah became poor in Asteraceae after 3 Ma.

NE trade winds intensified in West Africa after 2.53 Ma and during two short periods before that (~2.7 and 2.6 Ma) associated with the intensification of the Northern Hemisphere glaciations.

Supplementary data to this article can be found online at http://dx.doi.org/10.1016/j.palaeo.2014.09.023.

Acknowledgements

The study was financially supported by the Deutsche Forschungsgemeinschaft (DFG), grant DU221/5, and by the German Federal Administration for Education and Science (BMBF). FV thanks GLOMAR (Bremen International Graduate School for Marine Sciences). We are indebted to Susanne Jahns and Chiori Agwu for their help in the pollen analysis. We thank the Ocean Drilling Program for providing the samples. Alexus Wülbers, Walter Hale, Thomas Westerhold, Vera Lukies, and Ursula Röhl are acknowledged for helping with core handling, XRF scanning, and calibration of XRF data obtained during different sampling sessions. Mike Turner (Brunel University London) has kindly checked the English of the manuscript.

References

Arz, H., Pätzold, J., Wefer, G., 1999. The deglacial history of the western tropical Atlantic as inferred from high resolution stable isotope records off northern Brazil. Earth Planet. Sci. Lett. 167, 105–117.

Balsam, W.L., Otto-Bliesner, B.L., Deaton, B.C., 1995. Modern and last glacial maximum eolian sedimentation patterns in the Atlantic Ocean interpreted from sediment iron oxide content. Paleoceanography 10, 493–507.

Bartoli, G., Hönisch, B., Zeebe, R.E., 2011. Atmospheric CO_2 decline during the Pliocene intensification of Northern Hemisphere Glaciations. Paleoceanography 26, 1–14 (PA4213).

Bonnefille, R., 2010. Cenozoic vegetation, climate changes and hominid evolution in tropical Africa. Glob. Planet. Chang. 72, 390–411.

Bonnefille, R., Riollet, G., 1980. Pollens des savanes d'Afrique orientaleCentre National de la Recherche Scientifique Paris. (140 pp. 113pl.).

Bonnefille, R., Potts, R., Chalié, F., Jolly, D., Peyron, O., 2004. High-resolution vegetation and climate change associated with Pliocene *Australopithecus afarensis*. Proceedings of the National Academy of Sciences 101, pp. 12125–12129.

Bremer, K., 1994. Asteraceae, Cladistics & Classification. Timber Press, Portland Oregon (752 pp.).

Brierley, C.M., Fedorov, A.V., Liu, Z., Herbert, T.H., Lawrence, K.T., Lariviere, J.P., 2009. Greatly expanded tropical warm pool and weakened Hadley circulation in the Early Pliocene. Science 323, 1714–1718.

Clemens, S.C., 1999. An astronomical tuning strategy for Pliocene sections: implications for global-scale correlation and phase relationships. Phil. Trans. Math. Phys. Eng. Sci. 357, 1949–1973.

Cohen, K.M., Finney, S.C., Gibbard, P.L., Fan, J.-X., 2013. The International Chronostratigraphic Chart. Episodes 36, 199–204.

COHMAP, 1988. Climatic changes of the last 18,000 years: observations and model simulations. Science 241, 1043–1052.

Collins, J.A., Govin, A., Mulitza, S., Heslop, D., Zabel, M., Hartmann, J., Röhl, U., Wefer, G., 2013. Abrupt shifts of the Sahara–Sahel boundary during Heinrich stadials. Clim. Past 9, 1181–1191.

Contoux, C., Ramstein, G., Jost, A., 2012. Modelling the mid-Pliocene warm period climate with the IPSL coupled model and its atmospheric component LMDZ5A. Geosci. Model Dev. 5, 903–914.

De Schepper, S., Gibbard, P.L., Salzmann, U., Ehlers, J., 2014. A global synthesis of the marine and terrestrial evidence for glaciation during the Pliocene Epoch. Earth Sci. Rev. 135, 83–102.

deMenocal, P.B., 2004. African climate change and faunal evolution during the Pliocene–Pleistocene. Earth Planet. Sci. Lett. 220, 3–24.

deMenocal, P.B., Ruddiman, W.F., Pokras, E.M., 1993. Influences of high- and low-lattitude processes of African terrestrial climate: Pleistocene eolian records from equatorial Atlantic Ocean Drilling Program Site 663. Paleoceanography 8, 209–242.

deMenocal, P.B., Ortiz, J., Guilderson, T., Sarnthein, M., 2000a. Coherent high- and low-latitude climate variability during the Holocene warm period. Science 288, 2198–2202.

deMenocal, P.B., Ortiz, J., Guilderson, T., Adkins, J., Sarnthein, M., Baker, L., Yarusinsky, M., 2000b. Abrupt onset and termination of the African Humid Period: rapid climate responses to gradual insolation forcing. Quat. Sci. Rev. 19, 347–361.

Dupont, L.M., Agwu, C.O.C., 1991. Environmental control of pollen grain distribution patterns in the Gulf of Guinea and offshore NW-Africa. Geol. Rundsch. 80, 567–589.

Dupont, L.M., Leroy, S.A.G., 1995. Steps toward drier climatic conditions in northwestern Africa during the Upper Pliocene. In: Vrba, E.S., Denton, G.H., Partridge, T.C., Burckle, L.H. (Eds.), Paleoclimate and Evolution with Emphasis on Human Origins. Yale University Press, New Haven, pp. 289–298.

Etourneau, J., Schneider, R., Blanz, T., Martinez, P., 2010. Intensification of the Walker and Hadley atmospheric circulations during the Pliocene–Pleistocene climate transition. Earth Planet. Sci. Lett. 297, 103–110.

Etourneau, J., Ehlert, C., Frank, M., Martinez, P., Schneider, R., 2012. Contribution of changes in opal productivity and nutrient distribution in the coastal upwelling systems to Late Pliocene/Early Pleistocene climate cooling. Clim. Past 8, 1435–1445.

Faugères, J.C., Legigan, P., Maillet, N., Latouche, C., 1989. Pelagic, turbiditic, and contouritic sequential deposits on the Cape Verde Plateau (Leg 108, Site 659, Northwest Africa): sediment record during Neogene time. In: Ruddiman, W.F., Sarnthein, M., et al. (Eds.), Proceedings ODP, Scientific Results 108, pp. 311–327.

Fedorov, A.V., Dekens, P.S., Mccarthy, M., Ravelo, A.C., deMenocal, P.B., Barriero, M., Pacanowski, R.C., Pilander, S.G., 2006. The Pliocene paradox (mechanisms for a permanent El Nino). Science 312, 1485–1489.

Fedorov, A.V., Brierley, C.M., Lawrence, K.T., Liu, Z., Dekens, P.S., Ravelo, A.C., 2013. Patterns and mechanisms of early Pliocene warmth. Nature 496, 43–49.

Gasse, F., 2000. Hydrological changes in the African tropics since the Last Glacial Maximum. Quat. Sci. Rev. 19, 189–211.

Govin, A., Holzwarth, U., Heslop, D., Ford-Keeling, L., Zabel, M., Mulitza, S., Collins, J.A., Chiessi, C.M., 2012. Distribution of major elements in Atlantic surface sediments (36°N–49°S): imprint of terrigenous input and continental weathering. Geochem. Geophys. Geosyst. 13, 1–23 (Q01013).

Hammer, Ø., Harper, D.A.T., Ryan, P.D., 2001. PAST: paleontological statistics software package for education and data analysis. Palaeontol. Electron. 4 (1), 1–9.

Haug, G.H., Sigman, D.M., Tiedemann, R., Pedersen, T., Sarnthein, M., 1999. Onset of permanent stratification in the subarctic Pacific Ocean. Nature 401, 779–782.

Haug, G.H., Ganopolski, A., Sigman, D.M., Rosell-Melé, A., Swann, G.A., Tiedemann, R., Jaccard, S.L., Bollmann, J., Maslin, M.A., Leng, M.J., Eglinton, G., 2005. North Pacific seasonality and the glaciation of North America 2.7 million years ago. Nature 433, 821–825.

Hennissen, J.A.I., Head, M.J., De Schepper, S., Groeneveld, J., 2014. Palynological evidence for a southward shift of the North Atlantic Current at ~2.6 Ma during the intensification of late Cenozoic Northern Hemisphere glaciations. Paleoceanography 29, 564–580. http://dx.doi.org/10.1002/2013PA002543.

Herbert, T.D., Cleaveland Peterson, L., Lawrence, K.T., Lui, Z., 2010. Tropical ocean temperatures over the past 3.5 million years. Science 328, 1530–1534.

Hooghiemstra, H., 1988. Palynological records from northwest African marine sediments: a general outline of the interpretation of the pollen signal. Philos. Trans. R. Soc. Lond. B 318, 431–449.

Hooghiemstra, H., Agwu, C.O.C., Beug, H.-J., 1986. Pollen and spore distribution in recent marine sediments: a record of NW-African seasonal wind patterns and vegetation belts. Meteor Forschungsergeb. C 40, 87–135.

Hooghiemstra, H., Bechler, A., Beug, H.-J., 1987. Isopollen maps for 18,000 yr BP of the Atlantic offshore of Northwest Africa: evidence for palaeo-wind circulation. Paleoceanography 2, 561–582.

Hooghiemstra, H., Lézine, A.-M., Leroy, S.A.G., Dupont, L., Marret, F., 2006. Late Quaternary palynology in marine sediments: a synthesis of the understanding of pollen distribution patterns in the NW African setting. Quat. Int. 148, 29–44.

Hutchinson, J., Dalziel, J.M., 1963. Flora of West Tropical Africa, II2nd. Millbank, London (544 pp.).

Jansen, E., Raymo, M.E., Blum, P., et al., 1996. Site 982 proceedings ODP initial reports 162. Ocean Drilling Program, College Station TX, pp. 91–138.

Jansen, J.H.F., van der Gaast, S.J., Koster, B., Vaars, A.J., 1998. CORTEX, a shipboard XRF-scanner for element analyses in split sediment cores. Mar. Geol. 151, 143–153.

Knapp, R., 1973. Die Vegetation von Afrika. Fischer, Stuttgart (626 pp.).

Kuechler, R.R., Schefuß, E., Beckmann, B., Dupont, L., Wefer, G., 2013. NW African hydrology and vegetation during the Last Glacial cycle reflected in plant-wax-specific hydrogen and carbon isotopes. Quat. Sci. Rev. 82, 56–67.

Laskar, J., Jouzel, F., Boudin, F., 1993. Orbital, precession, and insolation quantities for the Earth from −20 Myr to +10 Myr. Astron. Astrophys. 270, 522–533.

Lawrence, K.T., Liu, Z., Herbert, T.D., 2006. Evolution of the eastern tropical Pacific through Plio-Pleistocene glaciation. Science 312, 79–83.

Lawrence, K.T., Herbert, T.D., Brown, C.M., Raymo, M.E., Haywood, A.M., 2009. High-amplitude variations in North Atlantic sea surface temperature during the early Pliocene warm period. Paleoceanography 24, 1–15 (PA2218).

Lawrence, K.T., Sosdian, S.M., White, H.E., Rosenthal, Y., 2010. North Atlantic climate evolution through the Plio-Pleistocene climate transitions. Earth Planet. Sci. Lett. 300, 329–342.

Leroy, S.A.G., Dupont, L.M., 1994. Development of vegetation and continental aridity in northwestern Africa during the Late Pliocene: the pollen record of ODP 658. Palaeogeogr. Palaeoclimatol. Palaeoecol. 109, 295–316.

Leroy, S.A.G., Dupont, L.M., 1997. Marine palynology of the ODP Site 658 (N-W Africa) and its contribution to the stratigraphy of Late Pliocene. Geobios 30, 351–359.

Lézine, A.M., 1987. Paléoenvironnements végétaux d'Afrique occidentale nord-tropicale depuis 12000 BP. Thesis Université Aix-Marseille II, Marseille 180 pp.

Lisiecki, L.E., Raymo, M.E., 2005. A Pliocene–Pleistocene stack of 57 globally distributed benthic $\delta^{18}O$ records. Paleoceanography 20, 1–17 (PA1003).

Maher Jr., L.J., 1972. Nomograms for computing 0.95 confidence limits of pollen data. Rev. Palaeobot. Palynol. 13, 85–93.

Marlow, J.R., Lange, C.B., Wefer, G., Rosell-Melé, A., 2000. Upwelling intensification as part of the Pliocene–Pleistocene climate transition. Science 290, 2288–2291.

Moreno, T., Querol, X., Catillo, S., Alastuey, A., Cuecas, E., Herrmann, L., Mounkaila, M., Elvira, J., Gibbons, W., 2006. Geochemical variations in aeolian mineral particles from the Sahara–Sahel Dust Corridor. Chemosphere 65, 261–270.

Morley, R.J., 2000. Origin and Evolution of Tropical Rain Forests. Wiley, Chichester.

Mulitza, S., Prange, M., Stuut, J.-B., Zabel, M., von Dobeneck, T., Itambi, A.C., Nizou, J., Schulz, M., Wefer, G., 2008. Sahel megadroughts triggered by glacial slowdowns of Atlantic meridional overturning. Paleoceanography 23, 1–11 (PA4206).

Naafs, B.D.A., Stein, R., Hefter, J., Khélifi, N., De Schepper, S., Haug, G.H., 2010. Late Pliocene changes in the North Atlantic Current. Earth Planet. Sci. Lett. 298, 434–442.

Naafs, B.D.A., Hefter, J., Acton, G., Haug, G.H., Martínez-Garcia, A., Pancost, R., Stein, R., 2012. Strengthening of North American dust sources during the late Pliocene (2.7 Ma). Earth Planet. Sci. Lett. 317–318, 8–19.

Nicholson, S., 2009. A revised picture of the structure of the "monsoon" and land ITCZ over West Africa. Clim. Dyn. 32, 1155–1171.

Nicholson, S.E., Grist, J.P., 2003. The seasonal evolution of the atmospheric circulation over West Africa and Equatorial Africa. J. Clim. 16, 1013–1030.

Nicolás, J., Chiari, M., Crespo, J., Garcia Orellana, I., Lucarelli, F., Nava, S., Pastor, C., Yubero, E., 2008. Quantification of Saharan and local dust impact in an arid Mediterranean area by the positive matrix factorization (PMF) technique. Atmos. Environ. 42, 8872–8882.

O'Brian, C.L., Foster, G.L., Martínez-Botí, M.A., Abell, R., Rae, J.W.B., Pancost, R.D., 2014. High sea surface temperatures in tropical warm pools during the Pliocene. Nat. Geosci. 7, 606–611.

Peterson, L.C., Haug, G.H., Hughen, K.A., Röhl, U., 2000. Rapid changes in the hydrologic cycle of the tropical Atlantic during the Last Glacial. Science 290, 1947–1951.

Ravelo, A.C., Andreasen, D.H., Lyle, M., Olivarez Lyle, A., Wara, M.W., 2004. Regional climate shifts caused by gradual global cooling in the Pliocene epoch. Nature 429, 263–267.

Richter, T.O., van der Gaast, S., Koster, B., Vaars, A., Gieles, R., de Stichter, H.C., Haas, H. De, van Weering, T.C., 2006. The Avaatech XRF Core Scanner: technical description and applications to NE Atlantic sediments. Geochem. Soc. Spec. Publ. 267, 39–50.

Röhl, U., Abrams, L.J., 2000. In: Leckie, R.M., Sigurdsson, H., Acton, G.D., Draper, G. (Eds.), High resolution, downhole, and nondestructive core measurements from Site 999 and 1001 in the Caribbean Sea: application to the Late Paleocene thermal maximumProceedings ODP, Scientific Results 165. Ocean Drilling Program, College Station TX, pp. 191–203.

Ruddiman, W.F., Sarnthein, M., et al., 1987. Initial Reports of the DSDP/ODP, 108A. U.S. Governmental Printing Office Washington, pp. 657–668.

Ruddiman, W.F., Sarnthein, M., Backman, J., Baldauf, J.G., Curry, W., Dupont, L.M., Janecek, T., Pokras, E.M., Raymo, M.E., Stabell, B., Stein, R., Tiedemann, R., 1989. Late Miocene to Pleistocene evolution of climate in Africa and the low-latitude Atlantic: overview of Leg 108 results. In: Ruddiman, W.F., Sarnthein, M., et al. (Eds.), Proceedings ODP Scientific Results 108. Ocean Drilling Program, College Station TX, pp. 463–484.

Salzmann, U., Haywood, A.M., Lunt, D.J., Valdes, P.J., Hill, D.J., 2008. A new global biome reconstruction and data-model comparison for the Middle Pliocene. Glob. Ecol. Biogeogr. 17, 432–447.

Salzmann, U., Williams, M., Haywood, A.M., Johnson, A.L.A., Kender, S., Zalasiewicz, J., 2011. Climate and environment of a Pliocene warm world. Palaeogeogr. Palaeoclimatol. Palaeoecol. 309, 1–8.

Sarnthein, M., Tetzlaff, G., Koopmann, B., Wolter, K., Pflaumann, U., 1981. Glacial and interglacial wind regimes over the eastern subtropical Atlantic and North-West Africa. Nature 293, 193–196.

Sarnthein, M., Thiede, J., Pflaumann, U., Erlenkeuser, H., Fütterer, D., Koopmann, B., Lange, H., Seibold, E., 1982. Atmospheric and oceanic circulation patterns off Northwest Africa during the past 25 million years. In: von Rad, U., et al. (Eds.), Geology of the Northwest African Continental Margin. Springer, Heidelberg, pp. 545–604.

Scheuvens, D., Schütz, L., Kandler, K., Ebert, M., Weinbruch, S., 2013. Bulk composition of northern African dust and its source sediments — a compilation. Earth Sci. Rev. 116, 170–194.

Schulz, E., 1991. Paléoenvironnements dans le Sahara central Pendants l'Holocène. Palaeoecology of Africa 22, 191–202.

Schulz, M., Mudelsee, M., 2002. REDFIT: estimating red-noise spectra directly from unevenly spaced paleoclimatic time series. Comput. Geosci. 28, 421–426.

Stein, R., Haven, H.L., Littke, R., Rullkötter, J., Welte, D.H., 1989. Accumulation of marine and terrigenous organic carbon at upwelling Site 658 and nonupwelling Sites 657 and 659: implications for the reconstruction of paleoenvironments in the eastern subtropical Atlantic through late Cenozoic times. In: Ruddiman, W.F., Sarnthein, M., et al. (Eds.), Proceedings ODP Scientific Results 108. Ocean Drilling Program, College Station TX, pp. 361–385.

Steph, S., Tiedemann, R., Prange, M., Groeneveld, J., Schulz, M., Timmermann, A., Nürnberg, D., Rühlemann, C., Saukel, S., Haug, G., 2010. Early Pliocene increase in thermohaline overturning: a precondition for the development of the modern equatorial Pacific cold tongue. Paleoceanography 25, 1–17 (PA2202).

Tiedemann, R., 1991. Acht Millionen Jahre Klimageschichte von Nordwest Afrika und Paläo-Ozeanographie des angrenzenden Atlantiks: Hochauflösende Zeitreihen von ODP-Sites. Universität Kiel, pp. 658–661, (Thesis, 127 pp.).

Tiedemann, R., Sarnthein, M., Stein, R., 1989. Climatic changes in the western Sahara: aeolo-marine sediment record of the last 8 M.Y. (ODP-Sites 657–661). In: Ruddiman, W.F., Sarnthein, M., et al. (Eds.), Proceedings ODP Scientific Results 108. Ocean Drilling Program, College Station TX, pp. 241–277.

Tiedemann, R., Sarnthein, M., Shackleton, N.J., 1994. Astronomic timescale for the Pliocene Atlantic $\delta^{18}O$ and dust flux records of Ocean Drilling Program Site 659. Paleoceanography 9, 619–638.

Torrence, C., Compo, G.P., 1998. A practical guide to wavelet analysis. Bull. Am. Meteorol. Soc. 79, 61–78.

Trauth, M.H., Larrasoana, J.C., Mudelsee, M., 2009. Trends, rhythms and events in Plio-Pleistocene African climate. Quat. Sci. Rev. 28, 399–411.

Wara, M.W., Ravelo, A.C., Delaney, M.L., 2005. Permanent El Nino-like conditions during the Pliocene Warm Period. Science 309, 758–761.

Weltje, G.J., Tjallingii, R., 2008. Calibration of XRF core scanners for quantitative geochemical logging of sediment cores: theory and application. Earth Planet. Sci. Lett. 274, 423–438.

White, F., 1983. The vegetation of Africa. Natural Resources Research 20. UNESCO, 356 pp. 3maps.

Zabel, M., Schneider, R.R., Wagner, T., Adegbie, A.T., De Vries, U., Kolonic, S., 2001. Late Quaternary climate changes in Central Africa as inferred from terrigenous input to the Niger Fan. Quat. Res. 56, 207–217.

Zhang, Y.G., Pagani, M., Lui, Z., 2014. A 12-million-year temperature history of the tropical Pacific Ocean. Science 344, 84–87.